

Improved direction of arrival estimations with a wearable microphone array for dynamic environments by reliability weighting

Daniel A. Mitchell¹, Boaz Rafaely¹, Anurag Kumar²,
Vladimir Tourbabin²

¹School of Electrical and Computer Engineering, Ben-Gurion University
of the Negev, Israel.

²Reality Labs Research @ Meta, Menlo Park, USA.

Contributing authors: mitchdan@post.bgu.ac.il; br@bgu.ac.il;
anuragkr90@meta.com; vtourbabin@meta.com;

Abstract

Direction-of-arrival estimation of multiple speakers in a room is an important task for a wide range of applications. In particular, challenging environments with moving speakers, reverberation and noise, lead to significant performance degradation for current methods. With the aim of better understanding factors affecting performance and improving current methods, in this paper multi-speaker direction-of-arrival (DOA) estimation is investigated using a modified version of the local space domain distance (LSDD) algorithm in a noisy, dynamic and reverberant environment employing a wearable microphone array. This study utilizes the recently published EasyCom speech dataset, recorded using a wearable microphone array mounted on eyeglasses. While the original LSDD algorithm demonstrates strong performance in static environments, its efficacy significantly diminishes in the dynamic settings of the EasyCom dataset. Several enhancements to the LSDD algorithm are developed following a comprehensive performance and system analysis, which enable improved DOA estimation under these challenging conditions. These improvements include incorporating a weighted reliability approach and introducing a new quality measure that reliably identifies the more accurate DOA estimates, thereby enhancing both the robustness and accuracy of the algorithm in challenging environments.

Keywords: Direction-of-Arrival, Wearable arrays, Dynamic scenarios, LSDD algorithm

1 Introduction

Localizing multiple sound sources recorded with a microphone array in a reverberant environment is an important task in a wide range of applications, including robot audition and video conferencing. There is a wide range of direction-of-arrival (DOA) estimation algorithms available in the literature. These include beamforming [1], subspace methods such as multiple signal classification (MUSIC) [2], and algorithms based on time-delay of arrival estimation [3]. DOA estimation methods specifically developed for speech signals exploit the non-stationarity and sparsity of speech in the short-time Fourier transform (STFT) domain and enable DOA estimation even for under-determined systems with more sources than microphones [4, 5]. However, for noisy and reverberant environments, room reflections and additive noise mask the direct sound that carries DOA information, thus degrading the DOA estimation performance.

Recently, a general method for DOA estimation of multiple speakers that is robust against reverberation, has been developed [6, 7]. This method processes the signals in the time-frequency domain and employs a direct-path dominance (DPD) test [6–9] to identify time-frequency bins which are dominated by the direct path sound. This method has been widely studied [6, 7, 10–14] assuming a static environment, where both the sound sources and the microphone array are stationary. Among the algorithms using this method is the local space domain distance (LSDD) algorithm [9, 15, 16]. This is a computationally efficient algorithm which has proven successful for multi-speaker DOA estimation in static, noisy and reverberant environments. However, the DPD time-frequency algorithms, and specifically, the LSDD algorithm, have been less intensively studied in more realistic, dynamic environments where speakers and/or the microphone array are moving.

In dynamic environments, the motion of the sound sources and/or microphone array may lead to a rapid change of DOAs in time. Thus, accurately tracing the DOA of speakers requires short intervals between successive DOA estimates. Additionally, the DOA estimates may be smoothed in time using a tracking algorithm. Although DOA estimation and tracking algorithms in dynamic environments have been the subject of several recent studies [17–20], including studies presented as part of the Acoustic Source Localization and Tracking (LOCATA) [21–23] challenge, none of these have included experiments with wearable microphone arrays [24]. Such scenes are becoming increasingly more popular due to the increased interest in applications involving augmented reality [25].

In this article we address the problem of DOA estimation in a realistic scenario involving a wearable microphone array. The algorithm chosen for this work was based on the LSDD algorithm. As part of this effort we developed a framework for evaluating DOA estimates which change over time and for optimizing the many interdependent parameters in the DOA estimation algorithm. DOA estimates are obtained in short intervals for each active speaker to account for the rapid change in DOA. The DOA estimates were calculated using a subtractive weighted cluster algorithm, whose outputs include both the final DOA estimated within a time interval, and their corresponding estimation quality. Finally, we propose a reliability-weighted LSDD

algorithm for improved robustness under these challenging conditions. In summary, the contributions of this article are:

Development of a Novel Methodology for Increasing Robustness under Noisy and Dynamic Environments. The increased robustness is achieved by incorporating an array reliability measure and a cluster quality measure. The latter is integrated into a clustering algorithm that enhances the accuracy and robustness of the final DOA estimates within a time interval. The weighted reliability measure emerges from array characteristics and is also integrated into the DOA estimation algorithm. Both measures are detailed next.

Array Reliability measure. A mathematical model for analyzing the response of the microphone array steering vectors is described, generating a universal directivity map (UDM). The UDM provides an array-based reliability weight for each time-frequency DOA estimate. This reliability weight reflects the spatial selectivity of the array as a function of direction and frequency.

Cluster Quality measure. A novel quality measure is calculated for each final DOA estimate within a time interval. The quality measure is based on the relative weights of individual clusters, and is shown to be highly correlated with the DOA accuracy, therefore supporting an improved selection of a subset of accurate DOA estimates.

The experiments described in the article were performed using the Easy Communication (EasyCom) [26] dataset which was explicitly designed to represent a realistic cocktail-party environment. The proposed DOA estimation algorithm was found to have an improved performance on the EasyCom dataset while retaining the intrinsic speed and simplicity of the baseline LSDD algorithm.

2 Signal Model

In this section we discuss the mathematical model underlying the LSDD algorithm [15] for DOA estimation. Assume a microphone array comprising M microphones arranged according to some pre-defined configuration. Next, consider a sound field comprised of K plane waves generated by the same number of far-field sources, arriving from directions $\Psi_k, k \in \{1, 2, \dots, K\}$. These sources represent the direct sound from speakers in the scene, as well as reflections due to objects and room boundaries.

The signals captured by the microphones in the array transformed into the joint time-frequency domain by applying the short-time Fourier transform (STFT). This is done by first separating the speech signal into short time intervals of length δt . A fast Fourier transform (FFT) is then applied to each time segment. Following these pre-processing steps, the signal received by the m th microphone in time-frequency bin (t, f) can be described as

$$x_m(t, f) = \sum_{k=1}^K s_k(t, f)v_m(\Psi_k(t), f) + n_m(t, f), \quad (1)$$

where $v_m(\Psi_k(t), f)$ denotes the response of the m th microphone to a unit-amplitude plane wave at frequency f arriving from the k th source in direction $\Psi_k(t)$; $s_k(t, f)$ is the amplitude of the k th sound source signal; and $n_m(t, f)$ is the additive noise

present at the m th microphone. In writing Eq. (1) we have assumed the multiplicative transfer function property holds [27] and that $\Psi_k(t)$ is effectively constant within the duration of δt .

The corresponding complex signal received by the entire microphone array is thus

$$\begin{aligned} \mathbf{x}(t, f) &= [x_1(t, f), x_2(t, f), \dots, x_M(t, f)]^T, \\ &= \sum_{k=1}^K s_k(t, f) \mathbf{v}(\Psi_k(t), f) + \mathbf{n}(t, f), \end{aligned} \quad (2)$$

where

$$\begin{aligned} \mathbf{v}(\Psi_k(t), f) &= [v_1(\Psi_k(t), f), v_2(\Psi_k(t), f), \dots, v_M(\Psi_k(t), f)]^T, \\ \mathbf{n}(t, f) &= [n_1(t, f), n_2(t, f), \dots, n_M(t, f)]^T. \end{aligned} \quad (3)$$

3 DOA Estimation Baseline

In this section, the *baseline* LSDD algorithm for DOA estimation is described. This algorithm [7, 16, 28] has been recently developed, demonstrating computational simplicity and relative robustness to reverberation.

The essential element of the algorithm [15] is the directional spectrum $\mathbf{S}(t, f)$, which is defined for each time-frequency bin (t, f) over a grid of L directions $\phi_l, l \in \{1, 2, \dots, L\}$:

$$\mathbf{S}(t, f) = [S_1(t, f) S_2(t, f), \dots, S_L(t, f)]^T. \quad (4)$$

The components $S_l(t, f)$ are calculated by measuring the similarity between the vector $\mathbf{x}(t, f)$ and the vector $\mathbf{v}(\phi_l, f)$ (in the direction ϕ_l). Thus

$$S_l(t, f) = d(\mathbf{x}(t, f), \mathbf{v}(\phi_l, f)) \quad (5)$$

where $\mathbf{v}(\phi_l, f) = [v_1(\phi_l, f), \dots, v_M(\phi_l, f)]^T$ and $d(\mathbf{a}, \mathbf{b})$ denotes the similarity between two vectors \mathbf{a} and \mathbf{b} .

Originally, in the LSDD algorithm [15], $d(\mathbf{a}, \mathbf{b})$ was defined as

$$d(\mathbf{a}, \mathbf{b}) = \frac{1}{\min_{\beta} \left(\frac{\|\mathbf{a} - \beta \mathbf{b}\|}{\|\mathbf{a}\|} \right)}. \quad (6)$$

However, following [16] the more conventional cosine similarity measure is used:

$$d(\mathbf{a}, \mathbf{b}) = \frac{|\langle \mathbf{a}, \mathbf{b} \rangle|}{\|\mathbf{a}\| \|\mathbf{b}\|}, \quad (7)$$

where $\langle \mathbf{a}, \mathbf{b} \rangle$ denotes the inner product between \mathbf{a} and \mathbf{b} .

Given the spectrum $\mathbf{S}(t, f)$, the estimated DOA for the time-frequency bin (t, f) is defined as

$$\hat{\phi}(t, f) = \phi_{l_{\max}} , \quad (8)$$

where

$$l_{\max} = \arg \max_l (S_l(t, f)) . \quad (9)$$

By definition, the angle $\hat{\phi}(t, f)$ is measured *relative to the microphone array axis*. In this work, because arrays may move, the DOA is measured relative to an axis fixed to the room. In this case, the corresponding DOA estimate is denoted as $\hat{\theta}(t, f)$, where

$$\hat{\theta}(t, f) = \hat{\phi}(t, f) + \delta_{\text{array}} , \quad (10)$$

and δ_{array} is the angle between the microphone array axis and the axis fixed relative to the room.

Some of the bins (t, f) do not, however, contain a valid $\hat{\theta}(t, f)$ estimate. These are bins in which the direct signal from the speaker is masked by noise and/or reverberations. We may eliminate these bins by calculating a direct-path dominance (DPD) measure $\xi(t, f)$ for each bin (t, f) which we then test against a threshold λ . We use the binary function to identify “valid” bins:

$$V(t, f) = \begin{cases} 1 \text{ (“valid”)} & \text{if } \xi(t, f) \geq \lambda , \\ 0 & \text{otherwise ,} \end{cases} \quad (11)$$

There are various DPD measures available for identifying direct-sound dominant time-frequency bins [6–9]. The chosen DPD formula is as per [15]:

$$\xi(t, f) = \max_l (S_l(t, f)) . \quad (12)$$

In practice, following [29], the spectrum $\mathbf{S}(t, f)$ is smoothed before calculating $\hat{\theta}(t, f)$ and $\xi(t, f)$. The smoothed spectrum $\bar{\mathbf{S}}(t, f)$ is obtained by averaging $\mathbf{S}(t, f)$ in the range $t \in R_t$ and $f \in R_f$ around (t, f) .

Consideration is now given to how individual time-frequency estimates $\hat{\theta}(t, f)$ can be combined to provide accurate DOA estimates, first in a static environment and then in a dynamic environment.

3.1 DOA Estimation in a Static Environment

The problem of using the baseline LSDD algorithm for DOA estimation in a static environment is now considered. In such an environment, both the sound sources and the microphone array remain stationary. Under these conditions, accurate DOA estimates can be achieved by averaging the valid time-frequency DOA estimates $\hat{\theta}(t, f)$ over an extended period [15, 30].

Let us assume there are K speakers. The individual estimates $\hat{\theta}(t, f)$ are then clustered into K clusters [31]. Assuming a different cluster for each speaker, we may

generate a DOA estimate $\hat{\Theta}(k)$, $k \in \{1, 2, \dots, K\}$, for each speaker k by averaging the valid estimates $\hat{\theta}(t, f)$ for each cluster:

$$\hat{\Theta}(k) = \frac{1}{W_k} \sum_{(t,f)} \hat{\theta}(t, f) V(t, f) C_k(t, f), \quad (13)$$

where

$$W_k = \sum_{(t,f)} V(t, f) C_k(t, f), \quad (14)$$

$$C_k(t, f) = \begin{cases} 1 & \text{if } (t, f) \text{ belongs to the } k\text{th cluster,} \\ 0 & \text{otherwise,} \end{cases} \quad (15)$$

3.2 DOA Estimation in a Dynamic Environment

In this section, the problem of performing DOA estimation in a dynamic environment is considered. In such environments, where the positions of sound sources and/or the microphone array change over time, traditional long-term averaging of individual time-frequency DOA estimates is not feasible. This challenge arises from the necessity to continuously track the changing directions of sound sources. To accommodate these challenging conditions, the approach used in static scenarios requires modification.

The primary modification involves segmenting the time axis into short intervals, ΔT , during which the sound sources and microphone array can be considered approximately spatially constant. Each interval is labeled by its mid-time T , and the aim is to estimate a final DOA $\hat{\Theta}_T(k)$ for each active speaker k , defined as a speaker who is vocal during the interval T .

The application of the baseline LSDD algorithm for DOA estimation in a dynamic environment is now described. Fig. 1 shows the corresponding flow chart in the form of a block diagram. The main blocks in Fig. 1 are:

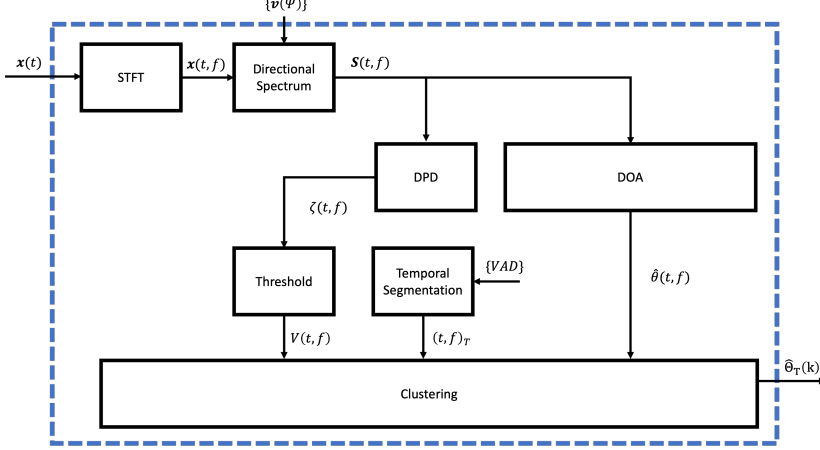


Fig. 1: Flowchart showing the main processing blocks for DOA estimation using LSDD-base algorithm in a dynamic environment.

- **STFT.** The microphone signals are transformed into the time-frequency domain using the short-time Fourier transform. The size of each time-frequency bin is denoted as $(\delta t, \delta f)$. Initially, a characteristic frequency range for the microphone array is defined as between f_{low} and f_{high} . Bins at frequencies outside this range are excluded from further processing. More details regarding the selection of f_{low} and f_{high} will be discussed in section 5.3.
- **Directional Spectrum \mathbf{S} .** The spectrum $\mathbf{S}(t, f)$ is calculated around each time-frequency bin (t, f) using Eq. (5). A smoothed spectrum $\bar{\mathbf{S}}(t, f)$ is calculated by averaging $\mathbf{S}(t, f)$ in the range $t \in R_t$ and $f \in R_f$ around (t, f) . Further details regarding the averaging will be discussed in section 6.3. The importance of smoothing the spectrum is shown in Ref. [29].
- **DOA Estimate $\hat{\theta}(t, f)$.** For each bin (t, f) , the DOA estimate is calculated using the smoothed spectrum $\bar{\mathbf{S}}(t, f)$ as in Eqs. (8) and (9).
- **DPD Measure $\xi(t, f)$.** For each bin (t, f) , the DPD measure $\xi(t, f)$ is calculated using the smoothed spectrum $\bar{\mathbf{S}}(t, f)$ in Eq. (12).
- **Threshold λ .** All bins (t, f) with DPD value $\xi(t, f)$ that exceed the threshold λ are identified. These bins are denoted as “valid” and are labeled $V(t, f) = 1$ (Eq. (11)).
- **Active Speech Time Segmentation.** The time axis is divided into intervals of length ΔT . If T denotes the mid-time of a given interval, then the interval T is classified as active if one or more speakers are speaking throughout the entire interval. In practice, the activity of T is provided by information from a voice activity detector (VAD).
- **Clustering .** All valid bins in the interval T are clustered. For each cluster k , the average DOA estimate $\hat{\Theta}_T(k), k \in \{1, 2, \dots, K\}$, is found (Eq. (13)).

4 Proposed DOA Estimation Algorithm

In this section, the proposed DOA estimation algorithm is described, incorporating two improvements to the baseline algorithm. First, a DOA reliability weight $w(t, f)$ for each time-frequency bin (t, f) is introduced. This allows DOA estimates that are more reliable to contribute more to the final DOA estimates. The reliability-weighted DOA estimate for the k th speaker is mathematically given by:

$$\hat{\Theta}(k) = \frac{1}{W_k} \sum_{(t,f)} w(t, f) \hat{\theta}(t, f) V(t, f) C_k(t, f), \quad (16)$$

where

$$W_k = \sum_{(t,f)} w(t, f) V(t, f) C_k(t, f), \quad (17)$$

The reliability weight w is discussed in Sect. 4.1.

Second, a quality measure $Q(k)$ for each cluster $k \in \{1, 2, \dots, K\}$ is introduced, assessing the likelihood that a cluster is a “true” cluster rather than a spurious one due to noise and interference. As will be demonstrated in Sect. 7, the quality measure is directly related to the expected accuracy of the final DOA estimates $\hat{\Theta}(k)$. Using $Q(k)$, DOA estimates with high accuracy can be selected, and less accurate estimates can be discarded. Alternatively, $Q(k)$ may be employed as a weight in a subsequent DOA tracking algorithm. The quality Q is discussed in Sect. 4.2.

We denote the new DOA algorithm as LSDD-wQ to emphasize that it incorporates a reliability weight $w(t, f)$ and a cluster quality Q .

4.1 DOA Reliability Weight w

The reliability weight $w(t, f)$ is modeled as a product of two reliability factors or functions:

- Data-based reliability $\xi(t, f)$. This function relies on the strength of the DPD measure $\xi(t, f)$ and represents the likelihood that the (t, f) bin is dominated by the direct-path.
- Array-based reliability α . This function measures the microphone directivity at any given look direction and frequency, calculated *directly* from the microphone array characteristics. The array-based reliability function does *not* change with the scenario and needs only to be computed once for each microphone array.

In calculating α it is supposed that it is a function of the estimated DOA $\hat{\phi}(t, f)$ and the frequency f . Thus, the reliability weight $w(t, f)$ can be expressed as:

$$w(t, f) = \alpha(\hat{\phi}(t, f), f) \times \xi(t, f). \quad (18)$$

Consider a specific steering vector $\mathbf{v}(\phi_h, f)$, corresponding to a frequency f and direction ϕ_h . The microphone array directivity for ϕ_h is then related to the similarity between $\mathbf{v}(\phi_h, f)$ and the set of steering vectors $\mathbf{v}(\phi_l, f), l \in \{1, 2, \dots, L\}$. This

calculation is repeated for all frequencies f yielding the following measure:

$$\Lambda_h(\phi_l, f) = d(\mathbf{v}(\phi_h, f), \mathbf{v}(\phi_l, f)) , \quad (19)$$

where Eq. (7) is used to compute $d(\mathbf{v}(\phi_h, f), \mathbf{v}(\phi_l, f))$. Physically $\Lambda_h(\phi_l, f)$ is related to the directivity of the microphone array at an angle ϕ_h .

In *deriving* the array-based reliability α we require $\alpha(\phi_h)$ to have a high value if $\Lambda_h(\phi_l)$ is high when $\phi_l \sim \phi_h$ and $\Lambda_h(\phi_l)$ is low elsewhere. We may implement this requirement using the directivity factor [32]. However, in practice, we found using the following mathematical model to be more robust.

First $\Lambda_h(\phi_l, f)$ is binarized using a predefined threshold thr :

$$B_h(\phi_l, f) = \begin{cases} 1 & \text{if } \Lambda_h(\phi_l, f) > thr , \\ 0 & \text{otherwise .} \end{cases} \quad (20)$$

Then, for each frequency f we count

- $m_h(f)$. This is the number of bins that are near ϕ_h . Physically $m_h(f)$ represents the concentration of Λ_h around the angle ϕ_h at the frequency f .
- $M_h(f)$. This is the number of bins that are far from ϕ_h . Physically $M_h(f)$ represents the number of outliers and sidelobes in Λ_h which are far from ϕ_h at the frequency f .

Mathematically, $m_h(f)$ and $M_h(f)$ are defined as follows:

$$m_h(f) = \sum_{|\phi_l - \phi_h| < \delta_{\text{near}}} B_h(\phi_l, f) , \quad (21)$$

$$M_h(f) = \sum_{|\phi_l - \phi_h| > \delta_{\text{far}}} B_h(\phi_l, f) \quad (22)$$

where δ_{near} and δ_{far} are, respectively, a small angle (≈ 10 deg) and a large angle (≈ 25 deg).

We now combine $m_h(f)$ and $M_h(f)$, in such a way that we emphasize frequencies which *simultaneously* have high $m_h(f)$ values and low $M_h(f)$ values. A method of doing this is to sort $m_h(f)$ over all frequencies f in ascending value and sort $M_h(f)$ over all frequencies f in descending value. We then add the corresponding indices, $r_h(f)$ and $R_h(f)$, in the sorted arrays:

$$\mathcal{R}_h(f) = r_h(f) + R_h(f) . \quad (23)$$

where $r_h(f) = l$ if $m_h(f)$ is the l th largest m_h value and $R_h(f) = l$ if $M_h(f)$ is the l th smallest M_h value.

We now normalize the $\mathcal{R}_h(f)$ values into a *universal directivity map* (UDM) Ξ . Let \mathcal{R}_{max} and \mathcal{R}_{min} , denote the corresponding maximum and minimum \mathcal{R} values. Then

$\Xi(\phi_h, f)$ is defined as the normalized rank

$$\Xi(\phi_h, f) = \frac{\mathcal{R}_h(f) - \mathcal{R}_{\min}}{\mathcal{R}_{\max} - \mathcal{R}_{\min}}. \quad (24)$$

The UDM is used directly as the array-based reliability function α . Thus:

$$\alpha(\hat{\phi}(t, f), f) = \alpha(\phi_h, f), \quad (25)$$

where (ϕ_h, f) is the point closest to $(\hat{\phi}, f)$.

4.2 Cluster Quality Q

The quality measure Q measures the likelihood that a cluster of a set of DOA estimates $\hat{\theta}(t, f)$ is a true cluster and not a spurious cluster due to noise or interference. Although the formula developed for Q is a general formula it takes on a particularly simple form when used with a subtractive clustering algorithm. In what follows we shall therefore assume the DOA estimates $\hat{\theta}(t, f)$ are clustered using a subtractive clustering algorithm [31].

The subtractive weighted cluster algorithm works *iteratively* such that one cluster is generated per iteration. The clusters are ordered according to their weight W_k (Eq. (17)), where $W_k > W_l$ if $l > k$. Assuming K active speakers are present (this information is provided by a Voice Activity Detector), the cluster algorithm runs for K iterations and the corresponding DOA estimates $\hat{\Theta}(k), k \in \{1, 2, \dots, K\}$, are calculated using Eq. (16).

Each estimate $\hat{\Theta}(k)$ is assigned a quality measure $Q(k)$ by comparing the weight W_k with the $(K + 1)$ th weight W_{K+1}

$$Q(k) = \frac{W_k}{W_{K+1}}. \quad (26)$$

The equation for the new quality measure is adopted from Lowe [33] who used similar reasoning to define keypoint quality in image registration. *Note:* to calculate $Q(k)$ we need to run the cluster algorithm for one more iteration, i. e. $(K + 1)$ iterations altogether.

The pseudo-code used for clustering the time-frequency estimates $\hat{\theta}(t, f)$ and estimating $\hat{\Theta}(k)$ and the quality $Q(k)$ is detailed in Alg. 1.

Algorithm 1 Subtractive Weighted Clustering for DOA Estimates and their Qualities

1: **for** each interval T **do**
 2: Initialize histogram $H(i)$ for $i \in \{-180, -179, \dots, +180\}$
 3: **for** each valid time-frequency bin (t, f) ($V(t, f) = 1$) **do**
 4: Identify the bin index i closest to $\hat{\theta}(t, f)$ such that:

$$|i - \hat{\theta}(t, f)| \leq 0.5$$

5: Increment the histogram at bin i by the weight of the bin:

$$H(i) \leftarrow H(i) + w(t, f)$$

6: **end for**
 7: **for** $k = 1$ to $K + 1$ **do**
 8: Sum the values of histogram $H(i)$ within a window for smoothing:

$$L(i) = \sum_{j=i-\delta}^{i+\delta} H(j)$$

9: Find the cluster center i_k where $L(i)$ is maximum
 10: Each valid (t, f) bin which lies within the window $(i_k - \delta, i_k + \delta)$ are assigned a cluster indicator function $C_k(t, f) = 1$ (Eq. (15)).
 11: Calculate the sum of weights for the k th cluster using Eq. (17).
 12: Calculate $\hat{\Theta}(k)$ using Eq. (16).
 13: Zero out histogram entries near i_k to prevent them effecting the next cluster:

$$H(j) = 0 \text{ for } j \in \{i_k - \delta, \dots, i_k + \delta\}$$

14: **end for**
 15: **for** $k = 1$ to K **do**
 16: Calculate the quality measure $Q(k)$ using Eq. (26)
 17: **end for**
 18: **end for**

We now summarize the equations underlying the new DOA estimation algorithm which we denoted as LSDD-wQ to emphasize it is jointly characterized by a reliability weight $w_{\text{new}}(t, f)$ and a quality measure $Q_{\text{new}}(k)$. For each cluster k the algorithm generates a DOA estimate $\hat{\Theta}_{\text{new}}(k)$ and a quality measure $Q_{\text{new}}(k)$:

$$\text{LSDD-wQ : } \begin{cases} \hat{\Theta}_{\text{new}}(k) &= \frac{1}{W_k} \sum_{(t,f)} w_{\text{new}}(t, f) \hat{\theta}(t, f) V(t, f) C_k(t, f), \\ Q_{\text{new}}(k) &= \frac{W_k}{W_{K+1}}, \end{cases} \quad (27)$$

where

$$\begin{aligned} w_{\text{new}}(t, f) &= \alpha(\hat{\phi}, f) \times \xi(t, f), \\ W_k &= \sum_{(t, f)} w_{\text{new}}(t, f) V(t, f) C_k(t, f). \end{aligned} \quad (28)$$

For convenience, the baseline LSDD algorithm (Eqs. (13) and (14)) is rewritten using the same notation. In the baseline algorithm, all time-frequency bins are assigned a uniform weight $w_{\text{base}}(t, f) = 1$ and all the clusters are assumed to be “true”, each with a quality measure $Q_{\text{base}} = 1$. Thus, for each cluster k , the baseline algorithm (denoted hereinafter as LSDD-base) generates a DOA estimate $\hat{\Theta}_{\text{base}}(k)$ and quality measure $Q_{\text{base}}(k)$:

$$\text{LSDD-base : } \begin{cases} \hat{\Theta}_{\text{base}}(k) &= \frac{1}{W_k} \sum_{(t, f)} w_{\text{base}}(t, f) \hat{\theta}(t, f) V(t, f) C_k(t, f), \\ Q_{\text{base}}(k) &= 1, \end{cases} \quad (29)$$

where

$$\begin{aligned} w_{\text{base}}(t, f) &= 1, \\ W_k &= \sum_{(t, f)} w_{\text{base}}(t, f) V(t, f) C_k(t, f). \end{aligned} \quad (30)$$

4.3 Proposed Algorithm for Dynamic Scenarios

In this section, the adaption of LSDD-wQ to a dynamic environment is considered. We follow the same approach described in Sect. 3.2. The corresponding flowchart is shown in Fig. 2. This represents a significant modification of the baseline flowchart shown in Fig. 1.

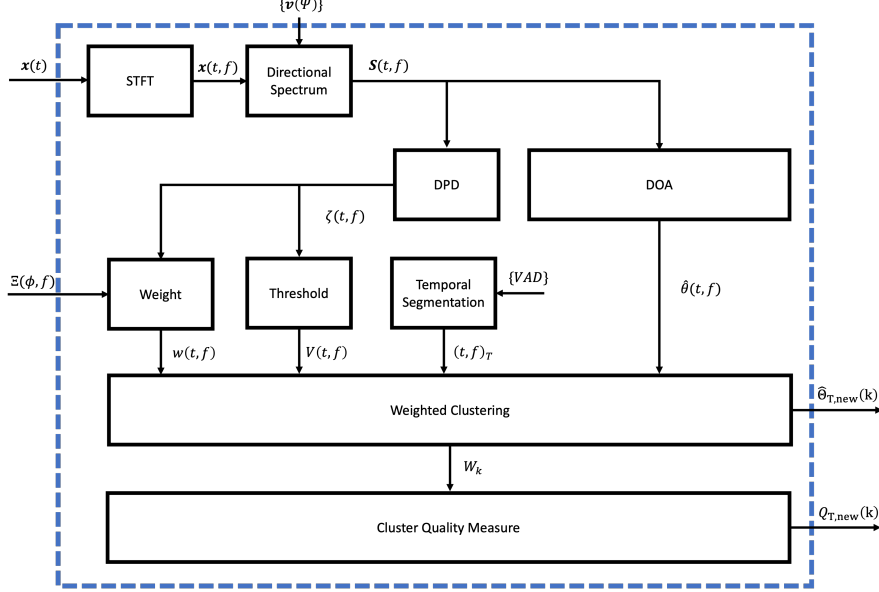


Fig. 2: Flowchart showing the main processing blocks for DOA estimation calculation in a dynamic environment using the LSDD-wQ algorithm.

Apart from the modules which appear in Fig. 1, the new flowchart in Fig. 2 includes three new signal processing modules. A list of these modules, together with a brief description of their content, is now given:

- **DOA Reliability Weight** $w_{\text{new}}(t, f)$. For each time-frequency bin, calculate a weight $w_{\text{new}}(t, f)$ which represents the reliability of its DOA estimate, using Eq. (28).
- **Subtractive Weighted Clustering**. For each active interval T , all valid bins, i.e. bins that satisfy $V(t, f) = 1$, are clustered by applying a *subtractive weighted* clustering algorithm (see Alg. 1). The output of the algorithm are a set of DOA estimates $\hat{\Theta}_{T,\text{new}}(k)$ (Eq. 27).
- **Cluster Quality Measure**. For each cluster $k, k \in \{1, 2, \dots, K\}$, found in time interval T , calculate a quality measure $Q_{T,\text{new}}(k)$ (Eq. 27).

5 Data and Array Analysis

In this section, the EasyComm dataset and the microphone array on which the DOA experiments were performed are presented, along with their characteristics. This characterization will support parameter selection for the algorithms.

5.1 The EasyComm dataset

The EasyComm dataset [26] incorporates a scenario with several speakers having a conversation, with the audio signals captured by augmented reality (AR) glasses equipped with an egocentric six-channel microphone array, worn by one of the conversation participants. Figure 3 shows a drawing of the glasses with locations of the microphones [26].

The dataset contains recordings of natural conversations in a noisy restaurant environment. Participants were equipped with close-talk microphones, a camera and tracking markers. They were asked to engage in conversations during several tasks, including introductions, ordering food, solving puzzles, playing games, and reading sentences. The recordings also contain an egocentric video viewpoint of the participants. The pose (position and rotation) of every participant was also recorded. The dataset was additionally labelled with annotators of voice activity.

Altogether the dataset contains $nID \sim 346$ segments of approximately 1-minute duration. Each segment is given an index ID , $ID \in \{1, 2, \dots, nID\}$.



Fig. 3: Illustration of the AR glasses with locations of microphones [26]. Four of the microphones are fixed rigidly to the glasses and two of the microphones are placed in the user’s ears.

The signals recorded by the microphones were sampled at a rate of 48 kHz which were then down-sampled to 16 kHz. The recorded data was transformed into the STFT domain using a 1024 samples ($\simeq 64$ msec) Hann window with an overlap of 512 samples. The microphone signals in the STFT domain were employed as an input to the algorithms under study.

Three characteristic parameters of the EasyComm dataset and the microphone array that are important in the context of this work, are:

- **Time interval ΔT .** This is the time over which the scenario may be regarded as spatially static and is investigated in Sect. 5.2.
- **Effective Frequency Range $[f_{\text{low}}, f_{\text{high}}]$.** This is the effective frequency band over which the array presents high directivity but is also aliasing-free, and is analyzed in Sect. 5.3.

Before dynamic DOA experiments can be performed, it is necessary to optimally choose these parameters. This is detailed in the following sections.

5.2 Selection of Time Interval ΔT

The EasyCom dataset consists of $nID \sim 346$ segments of approximately 1-minute duration. Each segment is divided into intervals of length ΔT seconds. We classify each interval as “dynamic” if during this interval the change in ground truth position exceeds ζ degrees. Otherwise, the interval is “static”. Table 1 shows the percentage of “dynamic” intervals for different angles ζ and different interval durations ΔT . We see that the number of dynamic intervals is extremely low for all intervals $\Delta T \leq 500$ msec. The number of dynamic intervals increase somewhat at $\Delta T = 1000$ msec. although the percentage of dynamic intervals remains low. According to these considerations we chose $\Delta T = 500$ msec.

Table 1: Percentage of “dynamic” intervals for different change angles ζ and interval durations ΔT

ΔT (msec)	change angle ζ (deg)			
	3	5	7	10
100	00.0 %	00.0 %	00.0 %	00.0 %
300	00.6 %	00.1 %	00.0 %	00.0 %
500	02.4 %	00.5 %	00.1 %	00.0 %
1000	07.6 %	02.5 %	00.9 %	00.2 %
5000	30.6 %	17.0 %	09.0 %	03.5 %

5.3 Selection of Operating Frequency Range

The EasyCom dataset involves speech sound which naturally limits the frequency range of interest [34]. This frequency band may be further reduced in practice by aliasing effects which arise from the microphone array. The operating frequency range is found from the array directivity $\Lambda_h(\phi_l, f_k)$ (Eq. (19)).

Figure 4 shows Λ_h for look direction $\phi_h = 0^\circ$ and $M = 4$ microphones. Visual inspection shows that the preferred lower frequency is about $f_{low} = 1500$ Hz. For frequencies lower than this value, the directivity is too wide to be of any use. The situation for the upper frequency f_{high} is less clear-cut. For frequencies much greater than about 2500 Hz, there are side lobes which *may* degrade the spatial processing. This was investigated in a preliminary experiment. The final choice of f_{high} was 3500 Hz.

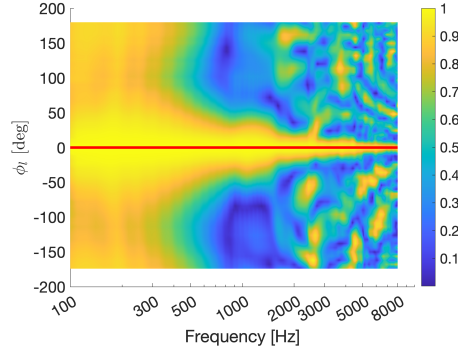


Fig. 4: Array directivity as measured by Eq. (19), with $\phi_h = 0^\circ$.

6 Preliminary Experiment for Parameter Selection

Several of the signal processing blocks in Fig. 2 have operating parameters which must be selected before DOA experiments can be performed. In this section, we show how these parameters were optimized. The parameters are:

- The filter parameters used for smoothing the spectrum $\mathbf{S}(t, f)$.
- The DPD threshold λ .

The experimental setup is given in section 6.1 and the methodology used to optimize the parameters is given in Sect. 6.2. The experimental results for each parameter are given in Sects. 6.3-6.4.

6.1 Experimental Setup

The operating parameters were experimentally optimized on the entire EasyComm dataset. This is described in Sect. 5.1.

6.2 Methodology

In optimizing the operating parameters we used two performance measures:

- **Absolute DOA Error** $\varepsilon(t, f)$. This is defined for each time-frequency bin (t, f) as the absolute difference between the true DOA $\Psi(t)$ and the estimated DOA $\hat{\theta}(t, f)$:

$$\varepsilon(t, f) = |\Psi(t) - \hat{\theta}(t, f)|, \quad (31)$$

Note: in Eq. (31) we have assumed that both $\Psi(t)$ and $\hat{\theta}(t, f)$ are measured with respect to the same coordinate system. In practice, $\Psi(t)$ is measured with respect to an axes defined relative to the room, while $\hat{\theta}(t, f)$ is measured with respect to the orientation of the eyeglasses. Thus, before calculating $\varepsilon(t, f)$, we transform $\hat{\theta}(t, f)$ to the fixed axes of the room by incorporating head tracking information.

- **Fraction of Low Error Bins** $n_{\text{low}}(T)$. This is defined for each active interval T as the fraction of valid bins with low errors:

$$n_{\text{low}}(T) = \frac{1}{N_{\text{val}}(T)} \sum_{(t,f)_T} L(t, f) V(t, f), \quad (32)$$

where

$$L(t, f) = \begin{cases} 1 & \text{if } \varepsilon(t, f) \leq 10^\circ, \\ 0 & \text{otherwise,} \end{cases} \quad (33)$$

$$N_{\text{val}}(T) = \sum_{(t,f)_T} V(t, f), \quad (34)$$

6.3 Time and Frequency Smoothing

Reference [29] have shown that it is beneficial to smooth the directional spectrum $\mathbf{S}(t, f)$ before calculating the DOA estimates $\hat{\theta}(t, f)$ and the DPD values $\xi(t, f)$.

For each bin (t, f) we smooth $\mathbf{S}(t, f)$ by averaging $\mathbf{S}(t, f)$ in the range $t \in R_t$ and $f \in R_f$ around (t, f) . $\bar{\mathbf{S}}(t, f) = [\bar{S}_1(t, f), \bar{S}_2(t, f), \dots, \bar{S}_L(t, f)]^T$ denotes the smoothed spectrum, with

$$\bar{S}_l(t, f) = \frac{1}{R_t R_f} \sum_{m=-r_t}^{r_t} \sum_{n=-r_f}^{r_f} S_l(t + m\delta T, f + n\delta f), \quad (35)$$

where $(\delta t, \delta f)$ is the size of STFT bin, $r_t = \lfloor (R_t/2) \rfloor$ and $r_f = \lfloor (R_f/2) \rfloor$.

Altogether we investigated four filters (listed in Table 2) corresponding to different combinations of (R_t, R_f) where U11 corresponds to no-smoothing.

Table 2: Smoothing Filters for $\mathbf{S}(t, f)$

Filter Name	R_t	R_f
U11	1	1
U33	3	3
U37	3	7
U57	5	7

Let \bar{n}_{low} denote $n_{\text{low}}(T)$ averaged over all data sessions and all time periods T . Then Fig. 5 shows how \bar{n}_{low} varies with λ for different smoothing filters. We see that \bar{n}_{low} increases significantly with λ . Inspection of \bar{n}_{low} shows large differences between the different smoothing filters for large λ . However, these differences tend to decrease as λ decreases. The final filter chosen was U37.

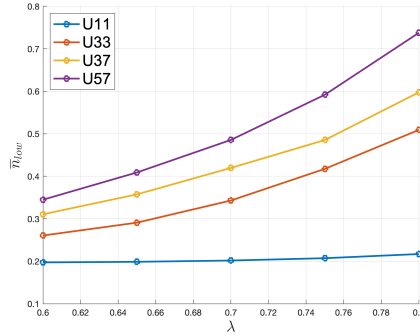


Fig. 5: Shows \bar{n}_{low} as a function of λ and for smoothing filters $U11$, $U33$, $U37$, $U57$.

6.4 DPD Threshold λ

In optimizing λ , our two principal requirements are:

- The probability Pr is high, where Pr is defined as the fraction of active intervals which contain at least one valid time-frequency bin (see Eq. (11)) to the total number of active intervals. Active intervals are defined as intervals for which one or more speakers are speaking throughout the interval.
- For most active intervals T the proportion of valid bins corresponding to direct sound leading to accurate DOA estimates is high. We may use the value of \bar{n}_{low} as an estimate of this proportion. The corresponding curves are shown in Fig. 5

Fig 6 shows how Pr varies with λ for several smoothing filters. We see that Pr decreases rapidly with λ . Inspection of these curves show a suitable value for λ is $\lambda = 0.7$.

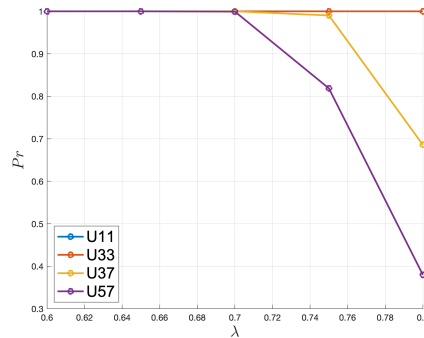


Fig. 6: Shows Pr as a function of λ for $\Delta T = 480$ msec and $f_{high} = 3500$ Hz. The curves were calculated for different smoothing filters.

7 DOA Estimation Experiments

In this section, DOA estimation results obtained with the EasyCom dataset using the new DOA estimation algorithm LSDD-wQ are presented. In particular, the focus is on measuring the differences in DOA performance between new and baseline algorithms as a result of using new weights $w_{\text{new}}(t, f)$ and a new quality measure $Q_{\text{new}}(k)$.

The experimental setup is described in Sect. 7.1. The methodology used is detailed in Sect. 7.2. Subsequently, in section 7.3, the experimental results obtained with the new DOA estimation algorithm are presented and compared with those obtained using the baseline algorithm.

7.1 Experimental Setup

Both the new and the baseline DOA algorithms were evaluated on the entire EasyCom dataset (Sect. 5.1).

7.2 Methodology

The performance of the DOA estimation algorithms in this dynamic environment, and specifically, their accuracy and robustness, are measured through a statistical analysis of the DOA estimates $\hat{\Theta}_T(k)$, their quality measures $Q_T(k)$ and their errors $E_T(k)$ for $k \in \{1, 2, \dots, K\}$. Here, $\hat{\Theta}_T(k)$, $Q_T(k)$ and $E_T(k)$ represent the final DOA estimate, the quality measure, and the absolute error of the k th active speaker in the interval T , respectively. With Ψ_k denoting the true DOA of the k th speaker in interval T , the absolute error is given by:

$$E_T(k) = |\hat{\Theta}(k) - \Psi_k|. \quad (36)$$

We compare the accuracy and robustness of the new and baseline DOA estimation algorithms as follows: for each algorithm we separately create a list of the absolute errors $E_T(k)$ and qualities $Q_T(k)$ for all T and k . From each list we select a subset of $P\%$ errors, which have the highest $Q_T(k)$ values. Then the mean absolute error of each subset is a measure of the estimation accuracy of the algorithm. Similarly, the relative number of outliers, which we define as absolute errors greater than 25° , is a measure of the robustness of the DOA algorithm.

In a subset containing $P\%$ errors, the mean absolute error obtained with the new algorithm is denoted as $\bar{M}_P(w_{\text{new}}, Q_{\text{new}})$. The corresponding mean absolute error obtained with the baseline algorithm is denoted as $\bar{M}_P(w_{\text{base}}, Q_{\text{base}})$. Likewise, $n_P(w_{\text{new}}, Q_{\text{new}})$ and $n_P(w_{\text{base}}, Q_{\text{base}})$ denote, respectively, the fraction of outliers in a subset containing $P\%$ errors obtained with the new and baseline algorithms.

For comparison purposes, the “ideal” mean absolute error for each P value is also presented. This ideal mean absolute error is calculated assuming an oracle which selects the subset with the *smallest* errors for each value of P . The corresponding “ideal” mean absolute errors obtained with the new and baseline algorithms are denoted as $\bar{M}_P(w_{\text{new}}, Q_{\text{ideal}})$ and $\bar{M}_P(w_{\text{base}}, Q_{\text{ideal}})$, respectively.

7.3 Results

In this section we compare the experimental results obtained with the new and baseline algorithms. We divide the section into three: starting with the relative accuracies of the two algorithms and then discussing the robustness of the algorithms. Finally, we discuss the relative contributions of w_{new} and Q_{new} .

Accuracy

Fig. 7 shows how the mean absolute errors $\overline{M}_P(w_{\text{new}}, Q_{\text{new}})$ and $\overline{M}_P(w_{\text{base}}, Q_{\text{base}})$ vary with P . We observe how, for all P , including $P = 100\%$, $\overline{M}_P(w_{\text{new}}, Q_{\text{new}})$ is *consistently* lower than $\overline{M}_P(w_{\text{base}}, Q_{\text{base}})$. Furthermore, we see that while the $\overline{M}_P(w_{\text{base}}, Q_{\text{base}})$ curve is relatively flat, the $\overline{M}_P(w_{\text{new}}, Q_{\text{new}})$ curve falls as P decreases. For example, at $P = 50\%$ the mean absolute error of LSDD-wQ drops to under 10° , while the corresponding baseline error remains relatively constant at about 20° .

We thus conclude that for all values of P the new algorithm LSDD-wQ is more accurate than LSDD-base with the relative accuracy of LSDD-wQ sharply increasing as we choose smaller values of P .

Robustness

Fig 8, shows how the fraction of outliers changes with P . We see clearly how for LSDD-wQ the fraction of outliers decreases sharply as P is reduced. For instance, at $P = 50\%$ the fraction of outliers drops to approximately 10%, while the fraction of outliers in the baseline algorithm remains relatively constant at around 27%.

We thus conclude that the new algorithm LSDD-wQ is substantially more robust than baseline algorithm LSDD-base.

Relative Contributions of w_{new} and Q_{new}

We now consider the relative contribution of the weights w_{new} and the quality measures Q_{new} in the new algorithm LSDD-wQ. For this purpose, we introduce two ‘‘combination’’ DOA algorithms:

- The first combination algorithm uses new weights $w_{\text{new}}(t, f)$ with baseline cluster quality $Q_{\text{base}}(k) = 1$. In this case, for each cluster k , we have a DOA estimate $\hat{\Theta}(k)$ and a quality measure $Q(k)$, where

$$\begin{cases} \hat{\Theta}(k) &= \hat{\Theta}_{\text{new}}(k) \\ Q(k) &= Q_{\text{base}}(k), \end{cases} \quad (37)$$

The mean absolute error of a subset $P\%$ obtained using this algorithm is $\overline{M}_P(w_{\text{new}}, Q_{\text{base}})$ and the corresponding fraction of outliers is $n_P(w_{\text{new}}, Q_{\text{base}})$.

- The second combination algorithm uses baseline weights $w_{\text{base}}(t, f) = 1$ with new cluster quality measures $Q_{\text{new}}(k)$. In this case, for each cluster k , we have a DOA estimate $\hat{\Theta}(k)$ and a quality measure $Q(k)$, where

$$\begin{cases} \hat{\Theta}(k) &= \hat{\Theta}_{\text{base}}(k) \\ Q(k) &= Q_{\text{new}}(k), \end{cases} \quad (38)$$

The mean absolute error of a subset $P\%$ obtained with this algorithm is $\bar{M}_P(w_{\text{base}}, Q_{\text{new}})$. The corresponding fraction of outliers is $n_P(w_{\text{base}}, Q_{\text{new}})$.

Fig. 9 shows how the mean absolute values obtained with the new, the baseline, and the two combination algorithms vary with P . In this figure we also show the “ideal” curves $\bar{M}_P(w_{\text{new}}, Q_{\text{ideal}})$ and $\bar{M}_P(w_{\text{base}}, Q_{\text{ideal}})$.

It is first observed that there is a natural ordering of the curves. For convenience we divide the curves into three pairs which we identify by coloring them red, green and blue. The red, green and blue curves, use, respectively baseline quality Q_{base} , new quality Q_{new} and ideal quality Q_{ideal} measures. However, each curve in the pair uses different weights. We use dashed lines to represent curves using baseline weights w_{base} and full lines to represent curves using the new weights w_{new} .

We see clearly that the baseline quality (red) curves lie above the new quality (green) curves which in turn lie above the ideal quality (blue) curves. Moreover, the difference in mean absolute value between the green and blue curves falls to about 5° as we decrease P while the difference in mean absolute value between the green and red curves reaches as much as 15° .

On the other hand, we clearly see for each pair of curves using the same quality measure, that the difference in mean absolute value is around $2 - 3^\circ$ or less.

We thus conclude that the new quality measure Q_{new} makes the largest contribution in improving the DOA accuracy of the LSDD-wQ algorithm. Moreover, as we reduce P the difference between curves representing the new quality measure and ideal quality measure fall to about 5° .

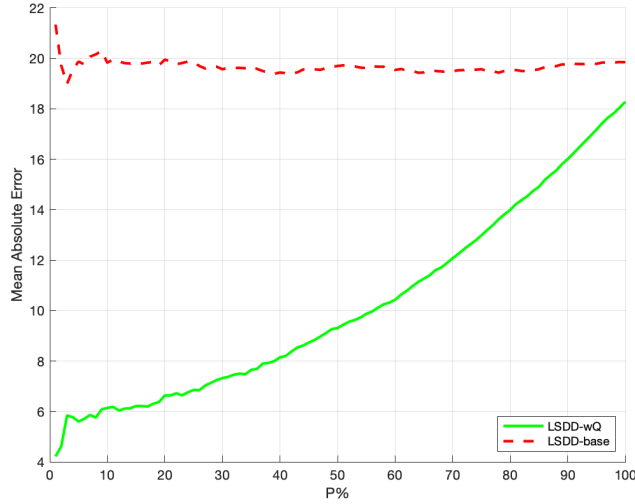


Fig. 7: Shows the mean absolute errors $\bar{M}_P(w_{\text{new}}, Q_{\text{new}})$ and $\bar{M}_P(w_{\text{base}}, Q_{\text{base}})$ as a function of $P\%$.

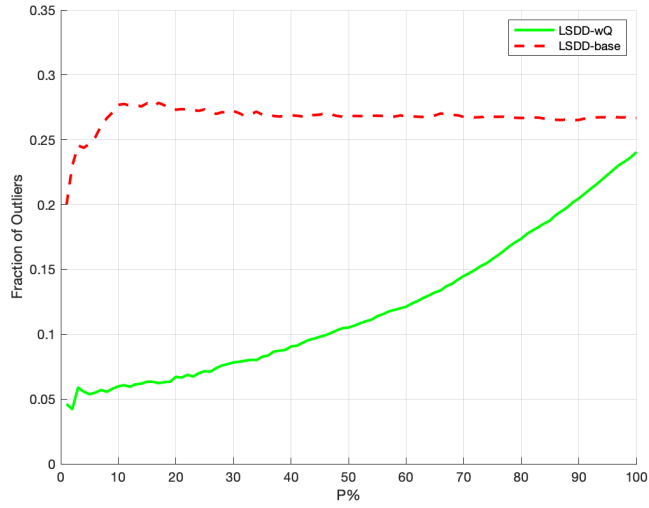


Fig. 8: Shows the fraction of outliers $n_P(w_{\text{new}}, Q_{\text{new}})$ and $n_P(w_{\text{base}}, Q_{\text{base}})$ as a function of $P\%$.

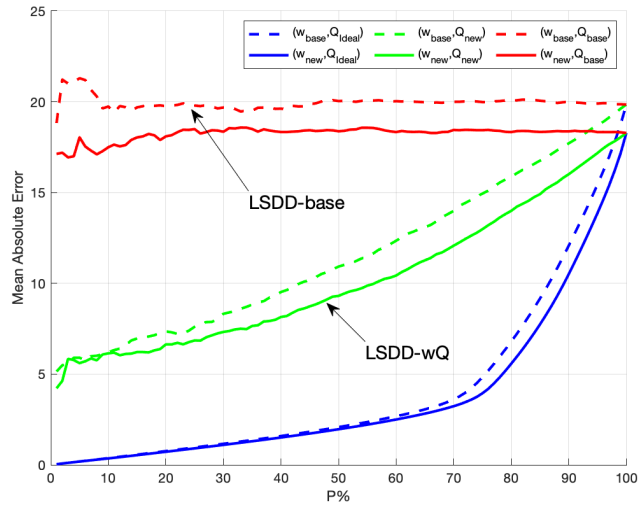


Fig. 9: Shows the mean absolute errors $\bar{M}_P(w_{\text{base}}, Q_{\text{base}})$, $\bar{M}_P(w_{\text{new}}, Q_{\text{base}})$, $\bar{M}_P(w_{\text{base}}, Q_{\text{new}})$, $\bar{M}_P(w_{\text{new}}, Q_{\text{new}})$, $\bar{M}_P(w_{\text{base}}, Q_{\text{ideal}})$ and $\bar{M}_P(w_{\text{new}}, Q_{\text{ideal}})$ as a function of $P\%$.

8 Conclusion

A detailed investigation into DOA estimation, particularly through algorithms based on LSDD, has been conducted. A novel methodology was described for performing DOA estimation in dynamic scenarios with wearable arrays. This included selection of an effective operating frequency range, developing a novel subtractive weighted clustering algorithm with quality measure for each cluster and giving each time-frequency estimate a reliability weight. The introduction of the new reliability weight gave a small, but consistent, improvement in DOA accuracy. The introduction of a cluster quality measure was found to be highly correlated with the DOA estimation accuracy. In particular, the cluster quality can be used to reduce outliers *before* tracking is undertaken. This in turn can make tracking algorithms both more accurate and robust.

9 Acknowledgement

This work was partially supported by Reality Labs Research @ meta

References

- [1] Van Veen, B.D., Buckley, K.M.: Beamforming: A versatile approach to spatial filtering. *IEEE ASSP Magazine* **5**(2), 4–24 (1988)
- [2] Schmidt, R.: Multiple emitter location and signal parameter estimation. *IEEE Transactions on Antennas and Propagation* **34**(3), 276–280 (1986)
- [3] Knapp, C., Carter, G.: The generalized correlation method for estimation of time delay. *IEEE transactions on acoustics, speech, and signal processing* **24**(4), 320–327 (1976)
- [4] Reju, V., Rashobh, R.S., Nguyen, A.H., Khong, A.W.: An efficient multi-source doa estimation algorithm for underdetermined system. In: 2018 16th International Workshop on Acoustic Signal Enhancement (IWAENC), pp. 86–90 (2018). *IEEE*
- [5] Brendel, A., Huang, C., Kellermann, W.: Stft bin selection for localization algorithms based on the sparsity of speech signal spectra. *ratio* **2**, 6 (2018)
- [6] Nadiri, O., Rafaely, B.: Localization of multiple speakers under high reverberation using a spherical microphone array and the direct-path dominance test. *IEEE/ACM Transactions on Audio, Speech, and Language Processing* **22**(10), 1494–1505 (2014)
- [7] Rafaely, B., Alhaiany, K.: Speaker localization using direct path dominance test based on sound field directivity. *Signal Processing* **143**, 42–47 (2018)
- [8] Hafezi, S., Moore, A.H., Naylor, P.A.: Multiple source localization using estimation consistency in the time-frequency domain. In: 2017 IEEE International

- Conference on Acoustics, Speech and Signal Processing (ICASSP), pp. 516–520 (2017). IEEE
- [9] Tourbabin, V., Rafaely, B.: Speaker localization by humanoid robots in reverberant environments. In: 2014 IEEE 28th Convention of Electrical & Electronics Engineers in Israel (IEEEI), pp. 1–5 (2014). IEEE
- [10] Moore, A., Evers, C., Naylor, P.A., Alon, D.L., Rafaely, B.: Direction of arrival estimation using pseudo-intensity vectors with direct-path dominance test. In: 2015 23rd European Signal Processing Conference (EUSIPCO), pp. 2296–2300 (2015). IEEE
- [11] Pavlidi, D., Delikaris-Manias, S., Pulkki, V., Mouchtaris, A.: 3d localization of multiple sound sources with intensity vector estimates in single source zones. In: 2015 23rd European Signal Processing Conference (EUSIPCO), pp. 1556–1560 (2015). IEEE
- [12] Delikaris-Manias, S., Pavlidi, D., Pulkki, V., Mouchtaris, A.: 3d localization of multiple audio sources utilizing 2d doa histograms. In: 2016 24th European Signal Processing Conference (EUSIPCO), pp. 1473–1477 (2016). IEEE
- [13] Madmoni, L., Rafaely, B.: Improved direct-path dominance test for speaker localization in reverberant environments. In: 2018 26th European Signal Processing Conference (EUSIPCO), pp. 2424–2428 (2018). IEEE
- [14] Beit-On, H., Rafaely, B.: Binaural Direction-of-arrival Estimation in Reverberant Environments Using the Direct-path Dominance Test. Universitätsbibliothek der RWTH Aachen, Germany (2019)
- [15] Tourbabin, V., Alon, D.L., Mehra, R.: Space domain-based selection of direct-sound bins in the context of improved robustness to reverberation in direction of arrival estimation. In: Proc. 11th European Congress and Exposition on Noise Control Engineering (EURONOISE18), pp. 2589–2596 (2018)
- [16] Mitchell, D.A., Rafaely, B.: Study of speaker localization under dynamic and reverberant environments. arXiv preprint arXiv:2311.16927 (2023)
- [17] Evers, C., Naylor, P.A.: Acoustic slam. *IEEE/ACM Transactions on Audio, Speech, and Language Processing* **26**(9), 1484–1498 (2018)
- [18] Wang, W., Wu, R.: High-dynamic doa estimation based on weighted l_1 minimization. *Progress In Electromagnetics Research C* **42**, 253–265 (2013)
- [19] Rusrus, J.: Moving sound sources direction of arrival classification using different deep learning schemes. PhD thesis, Université d’Ottawa/University of Ottawa (2023)

- [20] Hammer, H., Chazan, S.E., Goldberger, J., Gannot, S.: Dynamically localizing multiple speakers based on the time-frequency domain. *EURASIP Journal on Audio, Speech, and Music Processing* **2021**(1), 16 (2021)
- [21] Löllmann, H.W., Evers, C., Schmidt, A., Mellmann, H., Barfuss, H., Naylor, P.A., Kellermann, W.: The locata challenge data corpus for acoustic source localization and tracking. In: 2018 IEEE 10th Sensor Array and Multichannel Signal Processing Workshop (SAM), pp. 410–414 (2018). IEEE
- [22] Lebarbenchon, R., Camberlein, E., Di Carlo, D., Gaultier, C., Deleforge, A., Bertin, N.: Evaluation of an open-source implementation of the srp-phat algorithm within the 2018 locata challenge. *arXiv preprint arXiv:1812.05901* (2018)
- [23] Madmoni, L., Beit-On, H., Morgenstern, H., Rafaely, B.: Description of algorithms for ben-gurion university submission to the locata challenge. *arXiv preprint arXiv:1812.04942* (2018)
- [24] Zhao, J., Xu, Y., Qian, X., Wang, W.: Audio visual speaker localization from egocentric views. *arXiv preprint arXiv:2309.16308* (2023)
- [25] Carmigniani, J., Furht, B.: Augmented reality: an overview. *Handbook of augmented reality*, 3–46 (2011)
- [26] Donley, J., Tourbabin, V., Lee, J.-S., Broyles, M., Jiang, H., Shen, J., Pantic, M., Ithapu, V.K., Mehra, R.: Easycom: An augmented reality dataset to support algorithms for easy communication in noisy environments (2021) [arXiv:2107.04174](https://arxiv.org/abs/2107.04174) [cs.SD]
- [27] Avargel, Y., Cohen, I.: On multiplicative transfer function approximation in the short-time fourier transform domain. *IEEE Signal Processing Letters* **14**(5), 337–340 (2007) <https://doi.org/10.1109/LSP.2006.888292>
- [28] Anand, A., Mukul, M.K.: Comparison of stft based direction of arrival estimation techniques for speech signal. In: 2016 IEEE International Conference on Recent Trends in Electronics, Information & Communication Technology (RTEICT), pp. 200–205 (2016). IEEE
- [29] Beit-On, H., Tourbabin, V., Rafaely, B.: The importance of time-frequency averaging for binaural speaker localization in reverberant environments. In: INTERSPEECH, pp. 5071–5075 (2020)
- [30] Araki, S., Sawada, H., Mukai, R., Makino, S.: Doa estimation for multiple sparse sources with arbitrarily arranged multiple sensors. *Journal of Signal Processing Systems* **63**, 265–275 (2011)
- [31] Yager, R.R., Filev, D.P.: Generation of fuzzy rules by mountain clustering. *Journal of Intelligent & Fuzzy Systems* **2**(3), 209–219 (1994)

- [32] Beranek, L.L., Mellow, T.: *Acoustics: Sound Fields and Transducers*, 2nd edn. Academic Press, London (2012)
- [33] Lowe, D.G.: Distinctive image features from scale-invariant keypoints. *International journal of computer vision* **60**, 91–110 (2004)
- [34] Monson, B.B., Hunter, E.J., Lotto, A.J., Story, B.H.: The perceptual significance of high-frequency energy in the human voice. *Frontiers in Psychology* **5**, 587 (2014)